IEEE Access
Multidisciplinary | Rapid Review | Open Access Journal

Received April 22, 2018, accepted June 11, 2018, date of publication June 15, 2018, date of current version July 12, 2018.

Digital Object Identifier 10.1109/ACCESS.2018.2847634

Uniform Phase Empirical Mode Decomposition: An Optimal Hybridization of Masking Signal and Ensemble Approaches

YUNG-HUNG WANG[1], KUN HU[2], AND MEN-TZUNG LO[3,4]

[1]Research Center for Adaptive Data Analysis, National Central University, Taoyuan 32001, Taiwan
[2]Medical Biodynamics Program, Division of Sleep and Circadian Disorders, Brigham and Women's Hospital, Harvard Medical School, Boston, MA 02115, USA
[3]Graduate Institute of Translational and Interdisciplinary Medicine, National Central University, Taoyuan 32001, Taiwan
[4]Department of Biomedical Sciences and Engineering, National Central University, Taoyuan 32001, Taiwan

Corresponding author: Men-Tzung Lo (mzlo@ncu.edu.tw)

The work of Y.-H. Wang was supported by MOST of Taiwan under Grants 105-2221-E-008-051, 106-2221-E-008-023, and 106-2218-E-006-019. The work of K. Hu was supported by NIH under Grants R00-HL102241, R01AG048108-01A1, and P01AG009975. The work of M.-T. Lo was supported by MOST of Taiwan under Grants NSC 104-2314-B-002-200, NSC 104-3115-E-008-001, NSC 103-2321-B-008-003, NSC 103-2221-E-008-006-MY3, and NSC 102-2221-E-008-008.

ABSTRACT The empirical mode decomposition (EMD) is an established method for the time–frequency analysis of nonlinear and nonstationary signals. However, one major drawback of the EMD is the mode mixing effect. Many modifications have been made to resolve the mode mixing effect. In particular, disturbance-assisted EMDs, such as the noise-assisted EMD and the masking EMD, have been proposed to resolve this problem. These disturbance-assisted approaches have led to a better performance of the EMD in the analysis of real-world data sets, but they may also have two side effects: the mode splitting and residual noise effects. To minimize or eliminate the mode mixing effect while avoiding the two side effects of traditional disturbance-assisted EMDs, we propose an EMD-based algorithm assisted by sinusoidal functions with a designed uniform phase distribution with a comprehensive theoretical explanation for the substantial reduction of the mode splitting and the residual noise effects simultaneously. We examine the performance of the new method and compare it to those of other disturbance-assisted EMDs using synthetic signals. Finally numerical experiments with real-world examples are conducted to verify the performance of the proposed method.

INDEX TERMS UPEMD, EMD, uniform phase, mode splitting, residual noise.

I. INTRODUCTION

The empirical mode decomposition (EMD) [1] is a nonlinear, local [2] and adaptive method that decomposes a time series into a series of oscillatory components at different time scales, called intrinsic mode functions (IMFs). The IMFs at different time scales are recursively extracted, from fine to coarse, by applying a sifting process iteratively. In each sifting step, the local maxima (minima) are connected using cubic splines to form the upper (lower) envelope. The average of the upper and lower envelopes is then subtracted from the signal to get a new prototype IMF. The IMF is extracted after repeating the iterations several times. Except for the last IMF at the lowest frequency that represents the global trend of the input signal, each IMF has a well-behaved oscillatory property that often allows reliable assessment of instantaneous frequency and amplitude using Hilbert transform (HT) [1]. In addition, there is no assumption about the shape of each oscillatory component in the EMD. Thus, it is believed that each IMF of a physical or physiological signal derived from the EMD can better represent a specific underlying control process. The EMD has been successfully adopted in diverse fields such as biomedicine, geophysics, speech analysis, image analysis, and feature extraction, and has helped to reveal many physical and biological control mechanisms (e.g. [3]).

Despite the approved advantages of the EMD in terms of adaptivity, certain limitations can complicate the interpretation of the EMD results. Specifically, for data contain intermittency, the sifting process may detect extrema of the data belonging to different components at different time scales. As a result, the decomposed IMFs will consist of intermittent oscillatory components spanning a wide range

of disparate scales. This is known as the mode-mixing phenomenon [1], [4], which not only causes serious aliasing in the time-frequency distribution, but also obscures the physical meaning of individual IMFs.

A. RECENT WORK TO SOLVE MODE MIXING

To resolve these problems, there have been many proposed techniques including the noise-assisted EMD [5]–[8], the masking EMD [9]–[15], and the noise-assisted multivariate EMD (N-A MEMD) [16] that have attracted a lot of attention in recent years because of their superior performances in analyzing real world data.

Both the noise-assisted and masking EMD are based on the similar concept: applying certain disturbances to the raw data in order to obtain a perturbed signal with a more uniform distribution of extrema and to overcome the mode mixing problem. The noise-assisted EMD uses white noise as the disturbance. The method, named the ensemble EMD (EEMD), was first proposed by Wu and Huang [5]. This method first generated sets of perturbed signals, which were obtained by adding different realizations of white noise to the original data. Then, the EMD analysis is subsequently applied to these new data sets. Finally, the resultant IMFs are obtained by averaging the respective IMFs over different realizations.

In most cases, the EEMD has a better performance than the EMD in terms of mode-mixing and robustness. In parallel, Deering and Kaiser introduced the masking EMD in which sinusoids are used as the disturbance [9]. In each realization of the masking EMD, it decomposes the data into two IMFs, then the respective IMFs over the two (positive and negative sinusoids) realizations are averaged and noted as the resultant IMFs. The same procedure is recursively applied to the resultant IMF to extract the lower frequency components [9]. This approach improves the filtering characteristics of the EMD. However, one of the difficulties is that the frequency of corresponding physical components is sometimes not known beforehand.

Despite the great applications of the EEMD and the masking EMD to physiological/physical systems, they have noticeable shortcomings including mode splitting and residual noise effects that have been pointed out by Wu and Huang [5] for the EEMD and by Rilling and Flandrin [17] for the EMD.

B. MODE SPLITTING AND RESIDUAL NOISE

Mode splitting is the effect that the same oscillatory component at the same frequency or in a narrow frequency band resides in two or more neighboring IMFs, which would lead to underestimation of the amplitude of the oscillation, probably in a nonstationary way. This effect can be sometimes resolved by post-processing techniques such as recombination of the neighboring IMFs such that the resultant reconstructed IMF corresponds to the relevant physical component. The recombination procedure, however, is extremely difficult or sometimes impossible for a nonstationary signal. Mode splitting can be caused by two different factors (for a detailed discussion, see Sec. IV). First, the EMD can be interpreted locally as a filter (bank) [5], [6], [16], [18]–[20], by which an oscillatory component will be split into two different neighboring IMFs [5]–[6], [9], [17] when the frequency of the oscillation is in between the bandwidth of two filters. Second, the white noise is added to the signal in each realization. The decomposition may lead to a mode translation phenomenon [6] because of the stochastic nature of the white noise. In other words, the total number of IMFs and the number of the IMF corresponding to the true oscillation can be different for different realizations [7]. After taking the average of the respective IMFs in individual realizations to obtain the resultant IMFs, mode splitting may occur.

The second side effect is the residual noise. Historically, there are two definitions of the residual noise. The first definition is the reconstruction error or residual noise in the reconstruction of an original signal (defined in [5] and [6]), i.e., the input signal cannot be exactly reconstructed from the sum of the decomposed IMFs. The second definition is the residual noise (of the disturbance) in the individual IMF, and is noted as the RMS noise in [6]. In the EEMD, the amplitude of residual noise asymptotically approaches to zero as the number of realizations approaches to infinity. As compared to the EEMD, the residual noise effect is much more severe in the masking EMD, probably causing distorted waveforms or, even worse, incorrect IMFs (see more discussion below).

C. RECENT WORK TO SOLVE RESIDUAL NOISE

Recently a number of new noise-assisted EMD methods have been proposed to resolve the problem related to residual noise. Among them, the complementary EEMD (CEEMD) [6] is similar to the EEMD except that each assisted noise with plus and minus signs are applied in each realization such that the input signal is exactly reconstructed from the IMFs [1]. In the complete ensemble empirical mode decomposition with adaptive noise (CEEMDAN) [7], a particular noise is added at each stage of the decomposition and a unique residue is computed to obtain each IMF. The CEEMDAN reduces the mode-translation type mode splitting and the residual noise, and is complete. More recently, the improved CEEMDAN (ICEEMDAN) [8] based on the CEEMDAN is proposed to further reduce the residual noise in CEEMDAN. Moreover, Rehman and Mandic proposed the N-A MEMD [16] that is based on the multivariate EMD (MEMD) [21]. In the N-A MEMD, the signal in located at the first channel, and white noises are located at extra channels. Then the composite signal is decomposed using MEMD. The decomposed IMFs in the first channel are taken as the final results. Since the assisted noise does not interact with the signal directly, it is expected that the residual noise should be low.

In this study, first we express an IMF as the sum of attenuated copies of each tone plus the residual noise in the IMF for a synthesized signal consisting of (semi-) pure tones. Thus we can quantify and compare the mode splitting and residual noise obtained by different EMD-based methods. Understanding the origin of these effects will provide us the

hint for developing an improved algorithm. We then introduce the uniform phase EMD (UPEMD) method [22] — a disturbance-assisted EMD. More importantly, we provide a comprehensive theoretical explanation for the significant reduction of these two effects in the UPEMD based on the work of the Rilling and Flandrian [17]. Finally, we analyze the computational complexity of the UPEMD.

The remainder of the paper is organized as follows. In section II, we briefly review the EMD, EEMD and masking EMD. In section III, we investigate the mode splitting and residual noise effects associated with the disturbance-assisted EMD. In Section IV, we present the UPEMD method. In Section V, we analyze the computational complexity of the UPEMD. In Section VI, we present the experimental results on the nonlinear and the real world data to illustrate the efficacy of the proposed method and we conclude the paper with Section VII.

II. THE EMD, EEMD AND MASKING EMD APPROACHES

A. THE EMD ALGORITHM

The EMD is a local and adaptive method that decomposes a signal $x(t)$ into a finite number of IMFs and a trend (or residue). The EMD algorithm is briefly summarized below.

EMD Algorithm

1: Connect the local maxima/minima of $x(t)$ to obtain the upper/lower envelope using the cubic spline.
2: Derive the local mean of envelope, $m(t)$, by averaging the upper and lower envelopes.
3: Extract the temporary local oscillation $h(t) = x(t) - m(t)$.
4: If $h(t)$ satisfies some predefined stoppage criteria [5], $h(t)$ is assigned as an IMF noted as $c_m(t)$ where m is the IMF index. Otherwise set $x(t) = h(t)$ and repeat Step (1) – (3).
5: Compute the residue $r_m(t) = x(t) - c_m(t)$
6: Set $x(t) = r_m(t)$ and repeat steps (1) to (5) to extract the next IMF.

The fixed sifting number (n_s) as one of the stoppage criteria is adopted in this study. Note that it is also possible to use an ad hoc criterion to determine n_s adaptively, which is beyond the consideration of the current study. According to Huang *et al.* [1], an IMF should satisfy two conditions. (1) The local average is zero. (2) The number of extrema and zero-crossings differs at most by one. Equivalently the local maxima are all positive and local minima all negative [17]. Thus the Hilbert transform of an IMF often lead to meaningful instantaneous frequency and amplitude. The instantaneous amplitude versus frequency and time is noted as the Hilbert spectrum [1].

B. THE EEMD ALGORITHM

The EEMD algorithm first generates an ensemble of data sets obtained by adding different realizations of the white noise $w(t)$ to the input data $x(t)$. The EMD analysis is then applied to these new data sets $y(t)$. Denoting n_e and m as the number of realizations and the IMF index, respectively, the EEMD algorithm is briefly summarized below.

EEMD Algorithm

1: In each realization k, calculate the perturbed signal $y_k(t)$ by

$$y_k(t) = x(t) + \varepsilon_0 \cdot std(x(t)) \cdot w_k(t), \tag{1}$$

where ε_0 is the input noise amplitude, and *std* stands for the standard deviation.
2: Apply EMD with n_s iterations to decompose $y_k(t)$ into multiple IMFs.

$$y_k(t) = \sum_m c_{k,m}(t).$$

3: Repeat Step 1 and Step 2 using a different series of white noise.
4: The resultant IMF $c_m(t)$ is calculated as

$$c_m(t) = (1/n_e) \sum_{k=1}^{n_e} c_{k,m}(t) \tag{2}$$

The disturbance amplitude ε_0 is usually empirically chosen over the range of $\varepsilon_0 \approx 0.1 \sim 1.0$. The residual noise δ usually decays slowly as $\delta = (\varepsilon/\sqrt{n_e})$. In practice, n_e is often applied in the order of hundreds to achieve a compromise between accuracy and computational time.

C. THE MASKING EMD ALGORITHM

The masking EMD uses a sinusoid signal $w(t)$ as the assisted disturbance with its frequency f_w no less than that of the highest frequency component of the data. Then the EMD is applied to decompose the data $x(t)$ perturbed by $w(t)$ into two IMFs. The same procedure is repeated by applying the EMD to the data perturbed by $-w(t)$. Finally the average of the two resultant sets of IMFs is taken as the final result. Let $E_m(\cdot)$ be the operator, which produces the *mth* IMF decomposed by EMD [7]. The algorithm is summarized below:

Masking EMD Algorithm

1: Generate disturbance wave:

$$w(t;\theta) = \varepsilon \cdot \cos(2\pi f_w t + \theta) \tag{3}$$

2: Compute $c_1^+(t) = E_1(x(t) + w(t;\theta))$;
3: Compute $c_1^-(t) = E_1(x(t) + w(t;\theta+\pi))$
4: Obtain IMF1 by $c_1 = (c_1^+ + c_1^-)/2$, and IMF2 by

$$c_2 = x - c_1$$

In this method, the disturbance amplitude ε and phase θ of the assisted sinusoid signal are predetermined and the amplitude can be determined following the same rule used in EEMD or masking EMD [9], [10].

III. THE MODE SPLITTING AND RESIDUAL NOISE

In this section, we investigate and quantify the effects of mode splitting and residual noise on a synthesized signal of the combined (semi-) pure tones in the EEMD and the masking EMD.

We consider an input signal $x(t)$ consisting of multiple physical components. The signal is decomposed into a set of IMFs ($= n_{imf}$) by the disturbance-assisted EMD, in which the mode splitting effect manifests as the same physical component leaked into its neighboring IMFs. The residual noise is an artifact left in each individual IMF that is introduced by the decomposition of the perturbed signal. As a result, each IMF will consist of attenuated copies of the physical components plus the residual noise.

Here we measured the mode splitting and residual noise effects. Suppose $x(t)$ consisting of n_c tones that are defined by $p_j(t), j = 1 : n_c$. Suppose each tone $p_j(t)$ is leaked into all IMFs, which are stationary, then an IMF c_m contains a fragment of tone $\alpha_{jm} p_j(t)$ with α_{jm} the attenuation ratio of the *jth* tone onto IMF m. The attenuation ratio satisfies the identity, $\sum_{m=1}^{n_{imf}} \alpha_{jm} = 1$. Suppose an IMF c_m is contaminated by the residual noise δ_m, it yields

$$c_m(t) = \sum_{j=1}^{n_e} \alpha_{j,m} p_j(t) + \delta_m(t) \tag{4}$$

Equation (4) states that each IMF can be written as the summation of the attenuated copy of each tone plus the residual noise $\delta_m(t)$. Larger $||\delta_m(t)||$ implies more severe residual noise effect and vice versa. The mode splitting index (MSI_j) is defined as the percentage of the leakage of the amplitude of tone j into other IMFs, that is

$$MSI_j = 1 - \frac{\max_m(\alpha_{j,m})}{\sum_{m=1}^{n_{imf}} \alpha_{j,m}} = 1 - max_m(\alpha_{j,m}) \tag{5}$$

The MSI is bounded between 0 and 1. A larger MSI indicates a stronger mode splitting effect and vice versa. If $MSI = 0$, there is no mode splitting. The Fourier spectrum of the IMF $c_m(t)$ is applied to calculate the attenuation ratio α_{jm} of each tone and the residual noise in (4) even when the decomposed IMF is nonstationary. Then (5) is applied to calculate the MSI for each tone.

Example 1 (Two-Tone Signal With Intermittency):

The data $x(t) = x_H(t) + x_L(t)$, $0 \le t \le 1000$, is sampled at 1Hz rate. The subscript H and L are noted as the high and low frequency components, respectively, in this study. The signal $x_H(t)$ is an intermittent sinusoid with amplitude $a_H = 0.1$ and frequency $f_H = 1/8$, while $x_L(t)$ is a low frequency sinusoid with amplitude $a_L = 1$ and frequency $f_L = 1/240$. These signals are illustrated in the bottom right panel of Fig. 1(a). We first illustrate the mode mixing associated with EMD that is caused by intermittency, and how this phenomenon can be resolved using different disturbance-assisted EMD methods. The signal is decomposed by the EMD into 2 IMFs. In the EMD algorithm, the sifting process detects the extrema of $x_H(t)$ in some parts of the signal and detects the extrema of $x_L(t)$ for the remaining parts of the signal. Therefore the IMF1 obtained by EMD contains intermittent mixed mode, which consists of an intermittent high frequency wave riding on a low frequency wave. The decomposition of the signal obtained by the EEMD, CEEMD, ICEEMDAN, and masking EMD with $\varepsilon = 0.2$ and $n_s = 10$, are shown in Fig. 1(a). The frequency of the masking signal is set as $f_w = f_H$. The ICEEMDAN tool is provided by Colominas *et al.* [8]. For a fair comparison, the realization number n_e for CEEMD is taken to be $n_e/2$ since the plus and minus white noise is added in each realization.

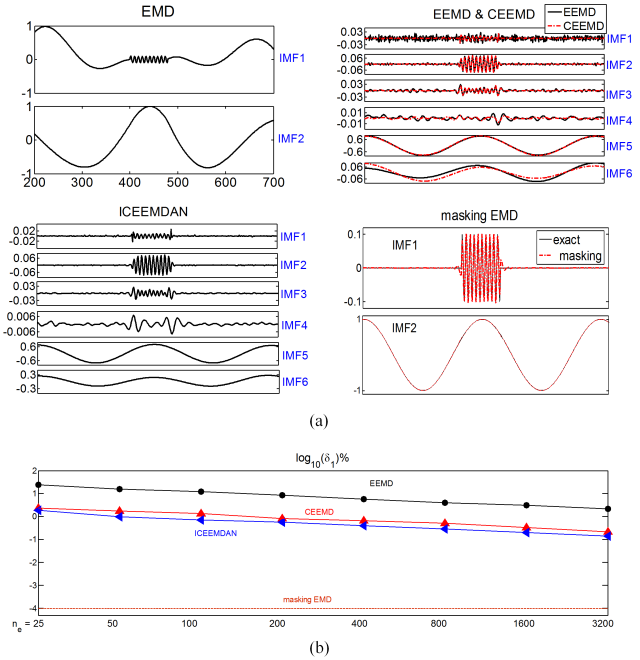

FIGURE 1. The two-tone signal with intermittency in Example 1. (a) top left: the IMFs by EMD; top right: the IMFs by EEMD/CEEMD; middle left: the IMFs by ICEEMDAN; middle right: the IMFs by masking EMD. All the results are conducted with $n_s = 10$, and the EEMD, CEEMD, and ICEEMDAN were conducted with $n_e = 200$. (b) The relative residual noise is represented in log10 base for the high-frequency components by different EMD-based methods.

TABLE 1. The *MSI* for example 1.

	EEMD	CEEMD	ICEEMDAN	Masking EEMD
MSI_H	0.18	0.20	0.20	0.00
MSI_L	0.08	0.08	0.27	0.00

As clearly shown in Fig. 1(a), the mode mixing is substantially reduced by the noise-assisted EMDs, but both of the components x_H and x_L are split into many IMFs by the EEMD, CEEMD, and ICEEMDAN. As can be observed in the figure, the two IMFs obtained by masking EMD, indeed, do not contain any recognizable mode mixing and mode splitting effect. The mode splitting index MSI_H and MSI_L by different disturbance-assisted methods are listed in Table 1.

Next, we measured the residual noise δ_H. In the EEMD, the IMF1 to IMF4 are recombined as the reconstructed high-frequency component IMF_H, and IMF5 to IMF6 as

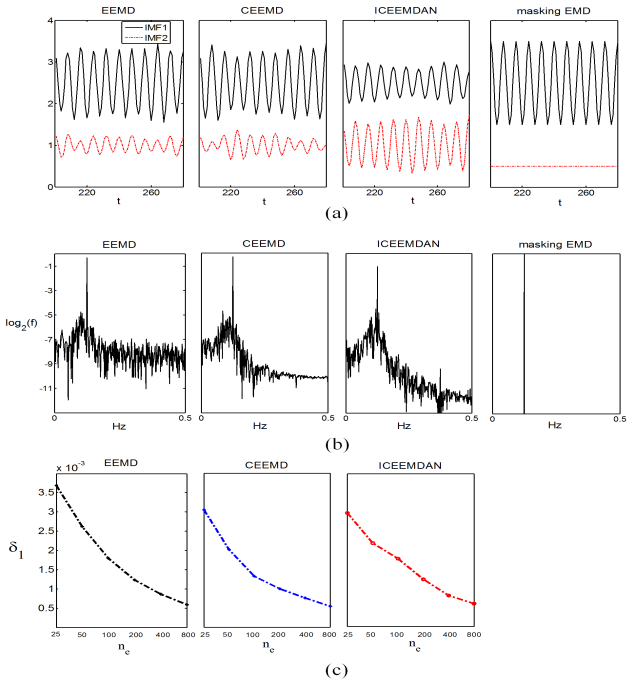

FIGURE 2. The decomposition of a one-tone signal in Example 2 by different disturbance-assisted EMDs with $n_s = 10$ and $\varepsilon = 0.3$. The EEMD, CEEMD, and ICEEMDAN are conducted with $n_e = 50$. (a) IMF 1 and 2 by different disturbance-assisted EMDs. (b) The log2 base Fourier spectrum of the IMF1. (c) The residual noise denotes as function of n_e. The residual noise of the masking EMD is almost zero and not shown.

the low-frequency components IMF_L. The IMF_H and IMF_L obtained by other noise-assisted methods are also recombined in a similar way. The relative residual noise is normalized as $\delta_{Hrel} = \|\delta_H\| / \|x_H\| \cdot 100\%$. To reduce the boundary effects, δ_{Hrel} is calculated in the interval between 580 and 780. The δ_{Hrel} as function of n_e with different methods are shown in Fig. 1(b). As expected, the residual noise for the noise-assisted methods decay slowly as n_e increases. In this example, the ICEEMDAN slightly outperforms the other noise-assisted methods, and the masking EMD outperforms all the noise-assisted methods.

Example 2 (A Pure Tone):

The one-tone signal seems simple but provides a good example to demonstrate the origin of mode splitting and residual noise in the disturbance-assisted EMDs. The IMF extracted by the EMD exactly represents the tone. However, if the tone is decomposed by the disturbance-assisted EMD, the tone will be separated into different IMFs — the mode splitting effect, and its waveform will be distorted by the residual noise. Understanding the undesired effects will provide us the hint for developing a better algorithm. Consider a pure tone with frequency $f = 1/8$Hz sampled at 1Hz. The signal is decomposed into 2 IMFs with $\varepsilon = 0.3$ and $n_s = 10$ by different EMD-based methods. The decomposed IMF 1 and 2 with $n_e = 50$ are shown in Fig. 2(a), and the *MSI*s are listed in Table 2. They indicate the presence of substantial mode splitting for all of the noise-assisted EMDs. The Fourier spectrum of IMF1 obtained by each disturbance-assisted EMD is shown

TABLE 2. The *MSI* for example 2.

	EEMD	CEEMD	ICEEMDAN	Masking EEMD
MSI	0.22	0.22	0.47	0.00

in Fig. 2(b). It is seen that the spectrum of the IMF1 obtained by the EEMD is broader than those by CEEMD and ICEEMDAN. However the frequency distributions of the spectral power obtained by different noise-assisted EMDs are all concentrated around the frequency of the tone (1/8Hz). Therefore, the residual noises do not differ significantly between different noise-assisted EMDs which can also be confirmed by Fig. 2(c). Note that the δ_1 decays gradually as n_e increases.

Next we investigate the IMFs obtained by the masking EMD. The frequency of the masking is set to be $f_w = f$. The δ_1 (not shown) and *MSI* in IMF1 presented in Table 2 are negligible with this particular masking frequency. This particular case, however, does not imply that the masking EMD is immune to residual noise. On the contrary, it sometimes generates deceptive frequency component as will be discussed in Sec IV.B.

IV. THE UNIFORM PHASE EMD (UPEMD)

As mentioned above, both the EEMD and the masking EMD can resolve the mode mixing phenomenon, but mode splitting and residual noise may occur consequently to deteriorate the decomposition performance. The residual noise in the EEMD results can be reduced by increasing the number of realizations. In the masking EMD, depending on the frequency and amplitude of the assisted sinusoid, the residual noise is sometimes much more severe than that in the EEMD. Particularly the deceptive frequency component generated by the masking EMD may lead to a wrong interpretation of the physics (will be discussed later). This effect must be suppressed to achieve reliable results. More insights into the EEMD and the masking EMD can be provided with the following considerations:

(1) The disturbance $w_k(t)$ can be expressed in the Fourier series as

$$w_k(t) = \sum_i a_{ki} \cos(2\pi f_i t + \theta_{ki})$$

Because the EEMD uses white noise as the assisted disturbance, the amplitude, the phase, and the frequency are all randomly distributed. The EEMD searches for all possible combinations of amplitude, phase and frequency of the perturbed signal in the sifting process such that the residual noise can be asymptotically cancelled out. The masking EMD, on the other hand, only searches for two phases of realizations with both the amplitude and the frequency predetermined. Therefore the EEMD suppresses residual noise better than the masking EMD does.

(2) (i)The masking EMD uses a narrow-band sinusoid as the disturbance while the EEMD (or noise-assisted EMD) uses the white noise as the disturbance which is a broad-band

signal containing many components over a wide range of frequencies. Frequency components of the disturbance signal and the input signal that have comparable frequency scales may "interact" with each other to produce mode splitting (see Fig. 2).

Therefore, the broad-band white noise obviously has high probability to interact with the input signal such that the EEMD, on average, produces more mode splitting than masking EMD.

(ii) EMD acts as an adaptive non-stationary filter bank. In the EEMD, the perturbed signal is rather stochastic, which may lead to somewhat random filter locations that a given frequency would not always be in the IMF of the same index. Even for an oscillatory signal at a fixed frequency, the IMF corresponding to the signal may have different indices in different realizations (mode translation). After obtaining the average of the corresponding IMFs, a mode-splitting effect occurs.

A. THE TWO-LEVEL UNIFORM PHASE EMD (UPEMD)

The masking EMD uses only two realizations of sinusoidal signals, which is insufficient to eliminate the residual noise effect. This observation suggests that a search for all the possible phases may help to minimize the residual noise. Here we present the two-level UPEMD to overcome the problems encountered in the disturbance-assisted EMD. Denote the number of phases as n_p with $n_p \in N, n_p > 1$. Let these n_p phases be uniformly distributed over the 2π space. Then the phase θ_k in the kth realization in (3) is calculated as

$$\theta_{\mathrm{k}} = 2\pi\ (k-1)\ /n_p, k = 1 : n_p \tag{6}$$

The two-level UPEMD is summarized in Algorithm 1.

Algorithm 1: Two-Level UPEMD (2L-UPEMD)

1: Assign $T_w(= 1/f_w)$, ε, and n_p.
2: Based on (6) and (3), calculated the perturbed signal $y_k\ (t)$ by

$$y_k\ (t) = x\ (t) + \varepsilon \cdot \cos\left(2\pi\left(f_w t + \frac{k-1}{n_p}\right)\right)$$

3: Perform the EMD to obtain the two IMFs, $c_{k,m}\ (\mathrm{t}) = E_m(x\ (t) + w(t; \theta_k)), m = 1, 2$
4: Repeat Steps 2 to 3 for $k = 1$ to n_p.
5: Obtain the resultant IMF1 and IMF2 as $c_m\ (t) = (1/n_p)\cdot \sum_k c_{k,m}\ (t)$

Notice that the masking EMD is a special case of the 2L-UPEMD with $n_p = 2$.

B. THE ONE-TONE PROBLEM

In this section, we will show that the mode splitting and residual noise can be reduced by increasing the number of phases in the 2L-UPEMD for the decomposition of a one-tone signal, which serves as the basis for analyzing complex signal, as will be discussed later. In each realization of the 2L-UPEMD, the perturbed signal $y\ (t)$ is the combination of the tone $x\ (t)$ and the assisted sinusoid $w_k\ (t)$ as denoted by

$$y_k\ (t) = a_w cos\ (2\pi f_w t + \varphi_w) + a_L cos\ (2\pi f_L t + \varphi_L) \tag{7}$$

For convenience, we also define the frequency ratio $f \triangleq f_L/f_w \leq 1$ and the amplitude ratio $a \triangleq a_L/a_w$. Since the frequency f_w of the assisted sinusoid is no less than that of the pure tone $x\ (t)$, the assisted sinusoid $w\ (t)$ is referred as the high-frequency component and the pure tone $x\ (t)$ is referred as the low-frequency component in this section. Note that this problem is equivalent to the decomposition of a two-tone signal by the EMD with the frequency of the assisted sinusoid being the high frequency signal. The numerical simulation with phase number $n_p = 1$, 2, and 16 are conducted respectively with $a_w = 1, f_w = 1/16$Hz, and $NS = 10$. The MSI and δ_1 for different f and a are displayed in Fig. 3. The MSI for $n_p = 16$ is displayed in Fig. 3(a). There are no significant differences in MSI between results with different phase numbers. The residual noise in IMF1 is presented in Fig. 3(b) and 3(c) for $n_p = 2$ and 16, respectively. For convenience, the residual noise is normalized based on the amplitude of the tone. As can be observed in these figures, the residual noise for the algorithm employing 16 phases is significantly lower than that of the algorithm employing 2 phases. The maximum residual noise is around 120% and 1% for the cases involving 2 and 16 phases, respectively.

Fig. 3 can be categorized into 3 regions based on the results of the numerical simulations: (A) $af < 1$; (B) $af^2 > 1$; (C) $af \geq 1 \& af^2 \leq 1$. Denote the extremum rate as the average number of extrema per unit length. The extremum rates in Regions A and B are constant and are equal to those of the high and the low frequency components, respectively. Region C is the transition region between Regions A and B, and the extremum rate is between those of the high and low frequency components. Furthermore, the extremum rate in most of Region C is non-uniformly distributed, especially near the boundary of Region B. Mode splitting occurs in Regions A and C, and the residual noise occurs in all regions.

The analytic solution of the IMFs decomposed by the EMD in Regions A and B can be obtained using an asymptotic theory [17]. The theory is based on two assumptions. First the spacing between the extrema in Regions A ($af \to 0$) and B ($af^2 \to \infty$) is constant. In fact, the average number of extrema per unit length (extremum rate) in Regions (A) and (B) is roughly constant despite the slightly non-uniform distribution of their extrema. Second the higher order aliasing error can be neglected. Here we analyze the decomposition in each region.

(1) Region A: $af < 1$.

The analytical solution for the decomposition of $x\ (t) + w_k\ (t)$ by EMD can be approximated by

$$c_{k,1}\ (t) = \cos\ (2\pi f_w t + \theta_k) + (1 - I\ (f))^{n_s} a \cos\ (2\pi f_L t + \phi_L) \tag{8}$$

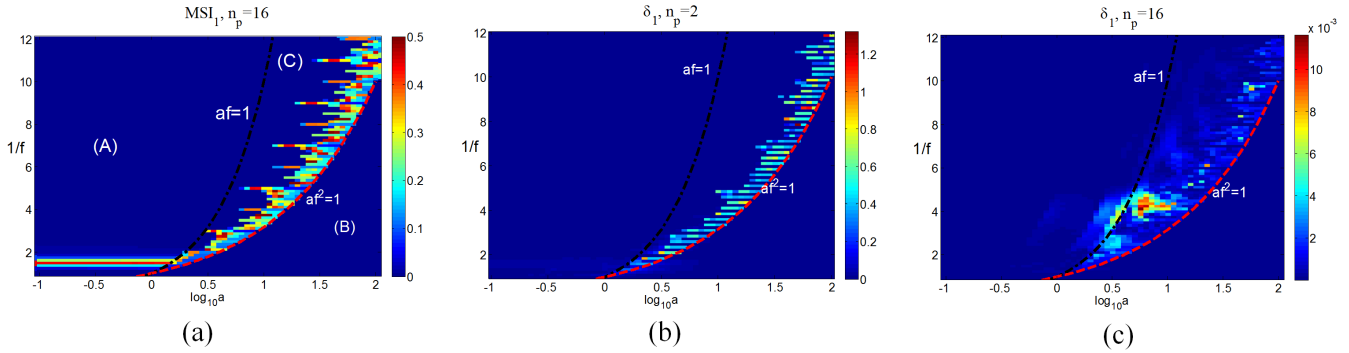

FIGURE 3. The mode splitting index (MSI_1) and the residual noise δ_1 obtained by the UPEMD for a one-tone signal. (a) MSI_1 with $n_p = 16$; (b) δ_1 with $n_p = 2$; (c) δ_1 with $n_p = 16$.

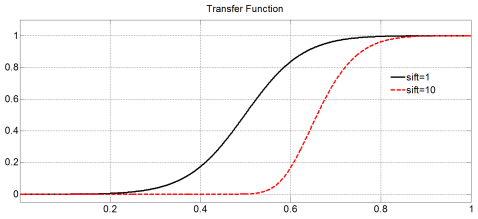

FIGURE 4. The transfer function $T(\tilde{f}) = 1 - I(\tilde{f})$ in (10) after one and 10 sifting.

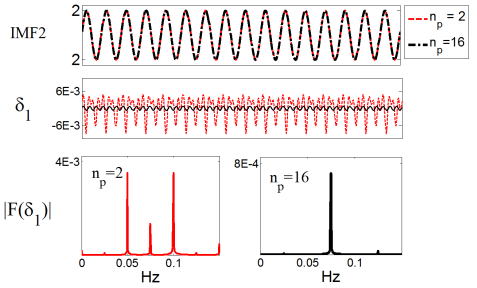

FIGURE 5. Decomposition of a one-tone signal using UPEMD with $n_p = 2$ and 16. The composite signal is located in Region A with $f_w = 1/16$Hz, $f = 0.4$Hz, and $a = 2$. Top panel: IMF2. Middle panel: residual noise. The bottom left and right panels show the Fourier spectra of the residual noises with $n_p = 2$ and 16, respectively.

The term $1-I(f)$ is the frequency response, and $I(f)$ is given by

$$I(f) = \left(\frac{\sin(\pi f)}{\pi f}\right)^4 \left(\frac{3}{2+\cos(2\pi f)}\right) \tag{9}$$

The resultant IMF1 of the 2L-UPEMD is obtained by averaging IMF1 $c_{k,1}$ over all realizations. The first term in (8) is cancelled out and IMF1 becomes

$$c_1(t) = (1 - I(f))^{n_s} a \cos(2\pi f t + \phi_L) \tag{10}$$

The second IMF c_2 is obtained by subtracting c_1 from the input signal. In (10), $T(f) = (1 - I(f))^{n_s}$ is the EMD equivalent filter and is an increasing function of f in [0, 1] as shown in Fig. 4. The mode splitting index for the tone is calculated as

$$MSI = \min\{T(f), 1 - T(f)\} \tag{11}$$

Equation (10) and (11) imply that MSI is unrelated to n_p and there is no significant residual noise in this region. Equation (10) states that the severity of mode splitting is a function of sifting number n_s, and that the frequency ratio f is independent of the amplitude ratio. We obtain $T(1) = 1$ when $f = 1$, in which the data is completely assigned to the IMF1 such that $MSI = 0$. This explains why the MSI_1 is almost zero when the masking frequency is equal to that of the (high) frequency component in Examples 1 and 2. On the other hand, if $f \to 0$, then $T(0) = 0$, i.e., the data is totally extracted into the IMF2, and $MSI = 0$. If $T(f)$ is greater than 1/2, then IMF1 contains more energy of the tone than IMF2 does, and vice versa.

We further examine the waveform of IMF1 and its corresponding Fourier spectrum with parameters $f = 0.4$Hz, $\varphi_L = -\pi/2$ and $a = 2$. The results are presented in Fig. 5. The MSI is 0.63% and 0.64% for $n_p = 2$ and 16, respectively. In these cases, no analytical expression of the residual noise can be found. Thus, the numerical simulation is conducted to calculate the residual noise. The L2 norm of the residual noises of IMF1 is 0.01% and 0.0014% for $n_p = 2$ and 16, respectively. These results show that the residual noise is significantly reduced using 16 phases. Noted that the mode splitting effect is a natural consequence of the EMD, but the effect is small for a two-tone signal with widely disparate scales.

(2) Region B: $af^2 > 1$.

In this region, the analytic solution for the two-tone signal decomposed by EMD is given by

$$c_{k,1}(t) = w_k(t) + x(t) - a_w \lambda_n \cos\left(2\pi f_r t + 2k_f(\phi_L) + \varphi_w\right) \tag{12}$$

In (12), $\lambda_n = 1 - T(f_r/f)$ and $2k_f - 1 < (1/f) < 2k_f + 1$, $k_f \in N$. The IMF $c_{k,1}$ consists of the perturbed signal $x(t)$ and the residual noise of frequency $f_r = 2k_f f - 1$. The amplitude λ_n and f_r are plotted in Fig. 6. As can been seen from this figure, λ_n lies in (0, 1) and $f_r < f$. The resultant IMF1 of the 2L-UPEMD is obtained by averaging the IMF1

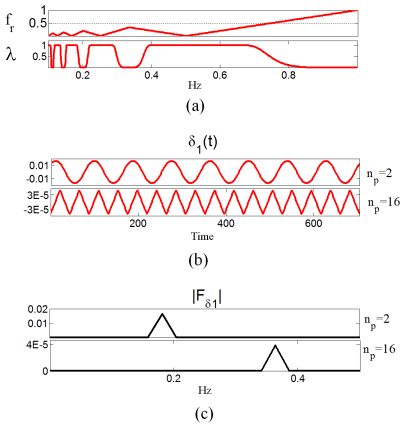

FIGURE 6. (a) λ_n versus f_r in (12). (b) The residual noise $\delta_1(t)$ using UPEMD with $n_p = 2$ and 16. (The composite signal is located in Region B with $f_w = 1/16$Hz, $f = 16/44$Hz, and $a = 10$.) (c) The corresponding Fourier spectrums of (b).

$c_{k,1}$ of all realizations:

$$c_1(t) = x(t) - (1/n_p)\sum_k \{a_w\lambda_n \cos\left(2\pi f_r t + 2k_f(\phi_L) + \varphi_{w,k}\right)\} \tag{13}$$

Equation (13) indicates that the resultant IMF1 is the sum of the tone and the residual noise $\delta_m(t)$ at frequency f_r. Note that there is no mode splitting in this region. The magnitude of the residual noise is proportional to the amplitude of the assisted sinusoid a_w. Based on the linear model, the residual noise is cancelled out if $n_p \geq 2$. This implies that the residual noise is low and its actual value can be obtained by numerical simulation. We further examined the waveform and its corresponding Fourier spectrums for the IMF1 with parameters $f = 16/44$Hz, $\varphi_L = 0$ and $a = 10$. The residual noise for $n_p = 2$ and 16 are shown in Fig. 6(b) and 6(c). The maximum residual noise of IMF1 are 1.6%, $1.1 \cdot 10^{-2}$%, $8.7 \cdot 10^{-3}$%, and $4.9 \cdot 10^{-3}$% for $n_p = 2$, 4, 8 and 16, respectively. These results demonstrate the superiority of the 2L-UPEMD in suppressing the residual noise. We notice that the frequency of the residual noise, f_r, is smaller than that of the data. When dealing with multi-component data, the residual noise acts as an error source and propagates into the subsequent IMFs. That is, the residual noise appears in the IMF at a scale (frequency) similar to that of the low frequency of the residual noise. Therefore, if a small n_p is adopted in the decomposition, the artifact component may be misinterpreted as a physically meaningful phenomenon.

(3) Region C: $af \geq 1 \& af^2 \leq 1$.

Because the extremum rate is non-uniformly distributed in most of this region, the EMD interprets the perturbed signal as the one with intermittency. Because there is no analytic solution in this region, the numerical simulation is conducted to calculate the mode splitting index and the residual noise. Here we investigate the tone with parameters $f = 16/27$Hz, $\varphi_L = 0$, and $a = 2$. The perturbed signal and its

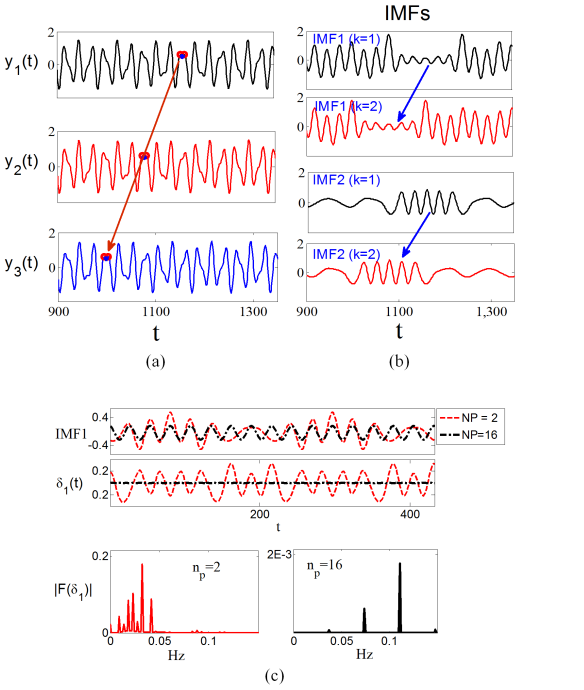

FIGURE 7. Analysis of the one-tone signal in Region C using UPEMD with different n_ps. The composite signal is located in Region C with $f_w = 1/16$Hz, $f = 16/27$Hz and $a = 2$. (a) The perturbed signal $y_k(t)$ with the subscript k as the realization index. (b) The IMF1 and IMF2 for $k = 1$ and 2 obtained by EMD. Mode mixing is obviously seen in the IMF1 and IMF2. (c) Top and middle panel: the IMF1 and the residual noise δ_1 profiles with $n_p = 2$ and 16, respectively; bottom panels: the corresponding Fourier transform of δ_1. The wide distributed spectrum using UPEMD with $n_p = 2$ indicating that the IMF1 is a physically incorrect component.

corresponding IMFs for the first few realizations are displayed in Fig. 7. The zone of the perturbed signal with high extremum rate, Z_h, is marked by the solid circles in the figure. Although the perturbed signal is periodic, the extremum rate is highly non-uniform in Region C. The decomposed IMF1 thus contains a mixing of small and large scales. As can be observed in the figure, the locations of the decomposed waves at small scales are close to zone Z_h and spread out slowly as the number of sifting increases. In the second realization, the zone Z_h is shifted to the left. The similar behavior remains in the subsequent realizations. After performing the average procedure in the 2L-UPEMD, the mode mixing and the residual noise phenomenon almost disappear. The decomposition results using 2 and 16 phases are presented in Fig. 7(d). The maximum residual noise $\delta_1(t)$ are 35% and 0.2% for $n_p = 2$ and 16, respectively. As expected, the case using 16 phases significantly reduces the residual noise. *MSI* is 19% in both cases, indicating that the mode splitting effect is insensitive to the phase number.

Although the one-tone signal appears to be over simplified, the results can serve as the theoretical basis for the analysis of the complex signals for the following reasons. Based on the recursive nature of the EMD, it is sufficient to consider the case that a signal can be decomposed into two IMFs.

Since the EMD is an algorithm with a high locality [2], we can focus on a short period of the signal, and classify each interval into any of the three regions (The extrema must be either uniformly distributed or non-uniformly distribution). This implies that the above approach can be readily extended to the analysis of signals with non-uniformly distributed extrema. Since the residual noise is substantially suppressed by increasing the number of phases in the 2L-UPEMD, it can be readily used to analyze the real world data containing multiple physical components.

C. THE MULTI-LEVEL UNIFORM PHASE EMD (UPEMD)

In this section, the 2L-UPEMD is extended to its multi-level version to deal with multicomponent data. The 2L-UPEMD is applied to decompose the data into two IMFs. The IMF1 is taken as the resultant IMF1, and IMF2 is treated as the new data. The same procedure is recursively applied to extract the resultant IMFs at lower frequencies.

The masking frequency f_w is predetermined by taking the dyadic property of EMD [5] that acts as an adaptive dyadic filter bank for the decomposition of the white noise with $n_s = 10$ [5], [18]. The number of resultant IMFs is approximately equal to $n_{imf} = \log_2 n$. The period with index m is determined as $T_w = 2^m$, $m = 1{:}\ \log_2 n$. For convenience, let $U_m(\cdot)$ be the operator which produces the *mth* IMF decomposed by 2L-UPEMD. The multi-level UPEMD algorithm is presented in Algorithm 2. The tool can be accessed at http://in.ncu.edu.tw/mzlo/drLo.html.

Algorithm 2: Multi-Level UPEMD

1: Assign n_p, set $n_{imf} = \log_2(n)$ and initial residue: $r_0(t) = x(t)$
2: Set $\varepsilon_m = \varepsilon_0 \cdot std(r_{m-1}(t))$, and $(T_w)_m = 2^m$
3: Perform the two-level UPEMD to obtain the IMF c_m (t), i.e. $c_m(t) = U_1(r_{m-1}; n_p, \varepsilon_m, (T_w)_m, n_s)$
4: Calculate residue $r_m(t) \leftarrow r_{m-1}(t) - c_m(t)$
5: Repeat Steps 2 to 5 for m= 1 ton_{imf} to extract all IMFs.

It is obvious that the input signal is exactly reconstructed from the IMFs.

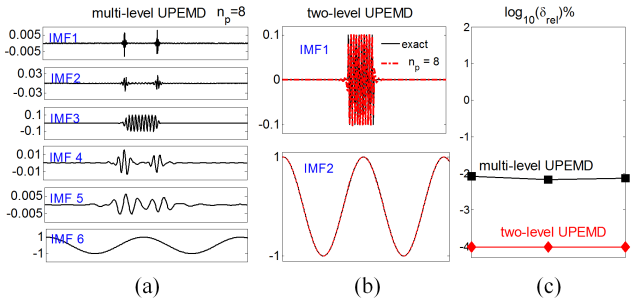

FIGURE 8. The decomposition of the signal in Example 1 using two-level and multi-level UPEMD with $n_s = 10$. (a) The IMFs by two-level UPEMD. (b) The IMFs by multi-level UPEMD with $n_P = 8$. (c) The relative residual noise in log10 base.

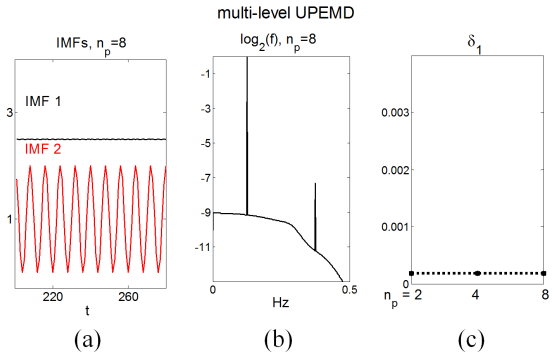

FIGURE 9. The decomposition of the signal in Example 2 using multi-level UPEMD. (a) IMF 1 and 2 (b) The log2 base Fourier spectrum of the IMF1. (c) The residual noise as function of n_P.

We tested the UPEMD using the signal in Example 1. The same parameters $\varepsilon = 0.2$ and $n_s = 10$ as in the noise-assisted methods were chosen for a fair comparison. The IMFs and the residual noises decomposed by two-level and multi-level UPEMD are displayed in Fig. 8. In the two-level UPEMD, the masking frequency f_w is assigned to be f_H. In the multi-level UPEMD, the IMF_H and IMF_L are reconstructed from the IMFs in the same manner as other noise-assisted EMDs. The mode splitting indices MSI_H and MSI_L are both insensitive to n_p. The values are 0.00 and 0.00, respectively, for the two-level UPEMD, and are 0.01 and 0 respectively, for the multi-level UPEMD. The UPEMD provides the least mode splitting effects compared to other noise-assisted methods as listed in TABLE 1. Moreover the performance of the two-level UPEMD is superior to that of the multi-level version as will be explained soon. The residual noise δ_{Hrel} for multi-level UPEMD are about 0.01%, which is at least an order of magnitude smaller than other noise-assisted methods even with n_e as large as 3200.

Second, we tested the multi-level UPEMD using the signal in Example 2. The same parameters $\varepsilon = 0.3$ and $n_s = 10$ were chosen for a fair comparison. The IMFs, spectrum, and the residual noise with $n_p = 8$ are presented in Fig. 9. The mode splitting index $MSI = 0.6\%$ and residual noise δ_1, are basically independent of n_p. They are smaller than all of the noise-assisted EMDs even with $n_e = 800$. Notice that the spectrum of the IMF1 in Fig. 9(b) shows a small third order harmonics residual error due to insufficient sample rate.

We made a remark on the UPEMD. In contrast to the EEMD, where noise with a fixed global amplitude is applied, the masking amplitude ε_m in step 2 can be determined adaptively for each level m. The selection of ε_m provides an extra level of adaptivity for the multi-level UPEMD which is similar to the (I)CEEMDAN methods [7], [8]. Moreover the masking frequency $(f_w)_m$ in step 3 is set a priori on a dyadic grid (i.e., increasing dyadically with m) that can also be determined adaptively for each level m.

Based on the recursive and local nature of EMD, Fig. 3 provides insights in determining value of ε_m and f_w to further reduce the value of the MSI and δ.

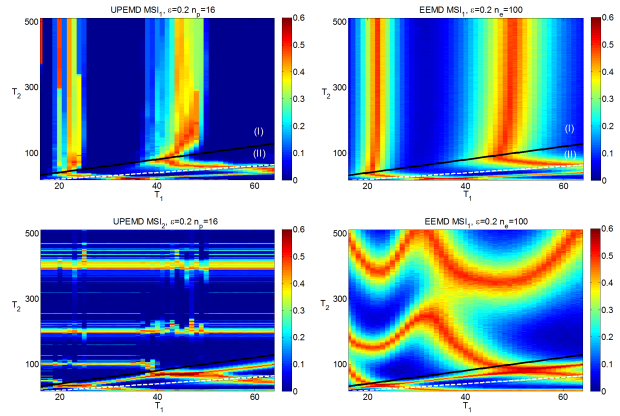

FIGURE 10. Analysis of the two-tone problem in Example 3. The mode splitting index MSI_1 and MSI_2 of a two-tone signal obtained by EEMD and UPEMD using different number of phases n_p. The black line represents $T_2 = 2T_1$, and the white dash line represents $T_2 = T_1$.

(a) To avoid the mode mixing, a sufficiently large ε_m (i.e. small a) can be applied such that $(a, 1/f)$ is located in Region (A) with low MSI. If the decomposition of the residue r_{m-1} produces no mode mixing effect, small or zero ε_m can be set such that $(a, 1/f)$ is located in Region (C) to minimize the mode splitting and residual noise side effects. For an illustration, the one-tone signal discussed earlier is decomposed using two-level UPEMD with $n_p = 2$ and parameters f = 16/44Hz, $\varphi_L = 0$ and $a = 10$. The EMD interprets the perturbed signal as the one with mode mixing because the extrema of the masking signal are not all "visible" in the perturbed signal (Fig. 7(d)). When a_w is large enough to guarantee that all its extrema are seen that corresponds to $af < 1$, the value of af will move horizontally from region (C) to (A) in Fig. 3(b). Thus the residual noise will be removed.

(b)The masking frequency f_w can be determined based on the Hilbert spectrum [9] or Fourier spectrum [10], [20] of the residue r_{m-1}. Here we propose a different approach. The optimized f_w can be determined based on Fig. 3. For instance, the MSI_H is about 1% for the signal in Example 1 decomposed by UPEMD with $f = f_w/f_H = 2$. If we set $f_w = f_H^+$ (i.e. slightly higher than the highest component in the signal), the MSI_H is reduced to almost zero.

Example 3 (Two-Tone Problem):

In this example, we examine the mode splitting effect when EEMD and the multi-level UPEMD are used to analyze a signal with two tones. The amplitudes of both tones in the signal are chosen to be both one, and their periods are noted as T_1 and T_2, respectively. The parameters adopted in the decompositions are $n_s = 10$, and $\varepsilon = 0.2$. The mode splitting indices for the two components, MSI_1 and MSI_2, are displayed in Fig. 10. These graphs can be roughly divided into two regions. In Region I, where $T_2 \geq 2T_1$, the two tones are well separated [9]. In Region II where $T_2 < 2T_1$, the two tones are strongly amplitude-modulated. For both methods the MSI_1 distribution in Region I mainly depends on the frequency (period) of tone 1 only. The MSI_2 for the EEMD in Region I depends on the frequencies of both tones. On the contrary, the MSI_2 for the UPEMD in Region I mainly depends on the period of tone 2. As the amplitude of disturbance increases, the MSI_2 in Region I would be more independent of T_1. The maximum MSI_2 is not much different between the two methods (i.e., 0.53 and 0.52 for the EEMD and the UPEMD, respectively). The mean value of MSI_2, as shown in TABLE 3, is significantly smaller in the UPEMD. In addition, the mean values of MSI_1 and MSI_2 are insensitive to the number of phases although the MSI distribution for the case using 16 phases is more regular than that using 2 phases (not shown).

TABLE 3. The average mode splitting index *MSI* for UPEMD and EEMD.

	MSI_1	MSI_2
EEMD, $\varepsilon = 0.2$	0.22	0.26
UPEMD, $\varepsilon = 0.2$, n_p=2	0.12	0.1
UPEMD, $\varepsilon = 0.2$, n_p=16	0.12	0.09

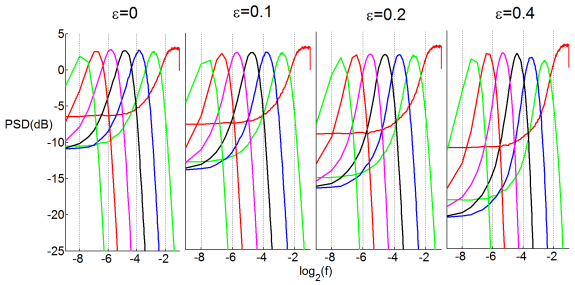

FIGURE 11. Dyadic filter bank structure of white noise in Example 4. Each figure plots the PSD versus normalized frequency.

Example 4 (Dyadic Filter Bank Structure):

In this example we investigate whether the filter bank structure [18] is preserved in UPEMD as in EMD. The Gaussian noise is decomposed by UPEMD using 4096 realizations with $n_p = 16$, length $n = 512$ and $n_s = 10$. In each realization, the Hamming window with no overlap is applied to calculate the power spectrum density (PSD). Then, the average over different realizations is taken as the final result. The PSD in dB versus normalized frequency in log2 base is shown in Fig. 11 with $\varepsilon = 0, 0.1, 0.2, 0.4$ respectively. Notice that UPEMD with $\varepsilon = 0$ is equivalent to the standard EMD. These figures show that the dyadic filter bank structure is preserved in UPEMD as occurred for the EMD/EEMD. The Fourier spectra of the decomposed IMFs (except for IMF1) from the standard EMD almost collapsed into a single curve [18] on the log-log plots except for the region around the very high frequency. It is worth mentioning that as ε increases, the UPEMD-derived IMFs show faster roll-off and narrowing bandwidth.

V. COMPUTATIONAL COMPLEXITY OF UPEMD

The computational complexity of the EMD [23] with data length n is given as $T_{EMD}(n) = 41 n_s \cdot n \log_2 n$ where the logarithm term is exactly the number of IMFs in the EMD

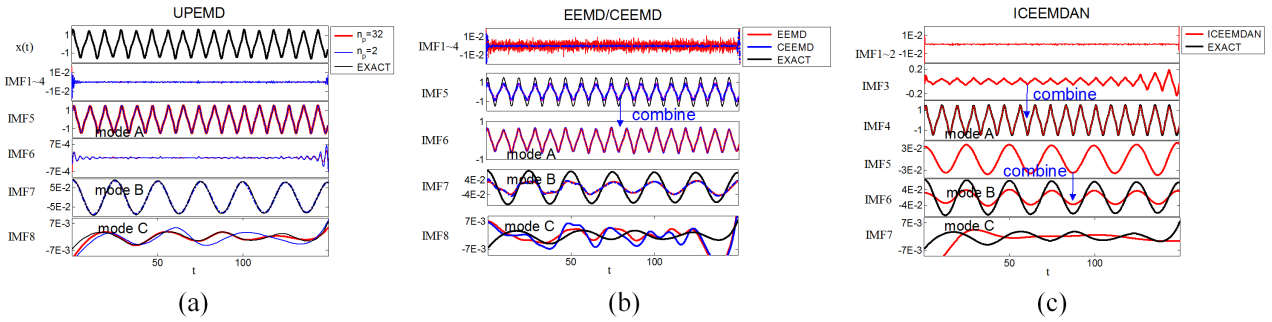

FIGURE 12. The decomposition of the signal $x(t)$ derived from the Duffing Equation in Example 5 using different EMD-based methods with $\varepsilon = 0.05$ and $n_s = 1000$. (a) The IMFs by UPEMD with $n_p = 2$ and 32. (b) The IMFs by EEMD/CEEMD with $n_e = 200$. (c) The IMFs by ICEEMDAN with $n_e = 200$. The black curves in (a) to (c) denote the IMFs obtained by EMD that serve as exact solutions.

TABLE 4. Computational complexity different versions of EMD.

Algorithm	Computational complexity
EMD	$41n_s \cdot n \log_2 n$
EEMD	$41n_e \cdot n_s \cdot n \log_2 n$
n_p phase UPEMD	$41n_p \cdot n_s \cdot n \log_2 n$;

decomposition, and the term $T_{sift}(n) = 41n_s \cdot n$ is the complexity of the sifting process. In the n_p-phase UPEMD, the number of extracted IMFs is $\log_2 n$, and the computational complexity in each IMF m is approximately equal to $n_p \cdot T_{sift}(n)$ and is listed in TABLE 4. In other words, the computational complexity of the n_p-phase UPEMD is n_p times that of the EMD. Based on our simulations in this study, $n_p = 4$ to 32 is sufficient to suppress most of the residual noise. The computational complexity of the n_p-phase UPEMD is much lower than that of the EEMD as can be observed in TABLE 4.

VI. NUMERICAL EXPERIMENTS FOR THE NONLINEAR AND REAL WORLD DATA

In this section we illustrate the performance of the UPEMD in analyzing nonlinear and real world signals. The *MSI* is estimated as follows. When the exact solutions of the physically components $p_i(t)$ are known. We need to modify (5) since it only holds for pure tones. Denoting IMF j as $\vec{c}_j$, the modified mode splitting index (*MMSI*) is defined as

$$MMSI_i = 1 - \max_j \frac{\vec{c}_j \cdot \vec{p}_i}{\left\|\vec{p}_i\right\|_2^2}, \quad 0 \le MMSI_i \le 1.$$

For real world nonstationary data, $p_i(t)$ is often unknown. The pseudo-*MSI* (*PMSI*) that is similar to the orthogonal index [1] is applied to estimate the mode splitting index between two adjacent IMFs as given by

$$PMSI_{i,i+1} = max\left(\frac{\vec{c}_i \cdot \vec{c}_{i+1}}{\left\|\vec{c}_i\right\|_2^2 + \left\|\vec{c}_{i+1}\right\|_2^2 + 10^{-8}}, 0\right)$$

As discussed in Sec. III. Larger *MMSI* and *PMSI* indicate more severe mode splitting.

TABLE 5. The *MMSI* in example 5.

Method\mode	mode A	mode B	mode C
UPEMD, $n_p = 32$	0.00	0.01	0.00
UPEMD, $n_p = 2$	0.00	0.03	0.06
EEMD	0.41	0.60	1.00
CEEMD	0.44	0.60	1.00
ICEEMDAN	0.05	0.56	1.00

Example 5 (Duffing Oscillator):

The nonlinear and nonstationary oscillator can be described by the Duffing equation:

$$\ddot{x}(t) = x - x^3 + 0.1\cos\left(2\pi t/25\right)$$

The oscillator with initial conditions $x(0) = \dot{x}(0) = 1$ has been previously studied using the EMD [1]. Here, we use this oscillator to examine the performances of different EMD-based methods with a special focus on mode splitting and residual noise, introduced by the two methods. The 4th order Runge-Kutta method is used to obtain the displacement $x(t)$ of Duffing oscillator. The top panel in Fig. 12(a) shows that the signal is nonstationary and the pattern of displacement never repeats. The EMD decomposes $x(t)$ into three physical modes, i.e., Modes A-C. Mode A corresponds to the intrinsic frequency of the system, which shows a strong intrawave frequency modulation. Mode B corresponds to a uniform intermediate frequency component representing the forcing function. Mode C represents a very low-intensity subharmonics. Because the amplitude of Mode C is much smaller than other modes, a slight mode splitting or residual noise effect would deteriorate its waveform and may obscure its physical meaning. The three IMFs show no mode mixing, and the frequencies of these 3 modes are well separated without mode splitting effects. Therefore the IMFs obtained by EMD will serve as the exact modes.

Here we present the decomposition results using different disturbance-assisted EMDs. We investigate the limitations and robustness of these algorithms by increasing disturbance amplitude slightly in each run until they fail in extracting the physical components of the data. First, we consider $\varepsilon = 0.05$. For the UPEMD with $n_p = 32$, IMF 1 to 4 and IMF 6 represent spurious residual noise modes that are

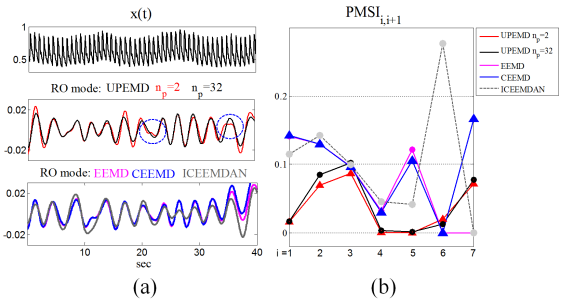

FIGURE 13. Analysis of blood flow velocity $x(t)$ in Example 6 using different disturbance-assisted EMDs with $\varepsilon = 0.4$ and $n_s = 10$. (a) Top panel: the signal $x(t)$; middle panel: the extracted RO mode by UPEMD with $n_p = 2$ and 32; bottom panel: the extracted RO mode by EEMD, CEEMD, and ICEEMDAN with $n_e = 200$. The points with positive local minima or negative local maxima are marked in the circles. The RO mode appears in IMF 6 for EEMD/CEEMD, and appears in IMF 7 for ICEEMDAN and UPEMD. (b) The *PMSI* values.

not associated with any physical component. The maximum amplitude of the residual noise of the combination of IMF 1 to 4 (neglecting the boundary effect) is about $5 \cdot 10^{-4}$ and that of component 6 is about $6 \cdot 10^{-4}$. The IMF 5, 7, and 8 match well with Mode A, Mode B, and Mode C, respectively. The *MMSI*s for different methods are shown in TABLE 5. It shows that the mode splitting effect is very weak in the UPEMD. The UPEMD with 2 phases is also performed and the result does not provide an IMF that can match Mode C well. For the EEMD/CEEMD with $n_e = 200$, the components 1 to 4 are not associated with any physical components but are just due to residual noise. The sum of these 4 IMFs shows that the maximum amplitude of the residual noise is about 0.01/0.0012, which is larger than that of the UPEMD. In addition, Mode A is split into IMFs 5 and 6. Mode B mainly occurs in IMF6. Mode C mainly occurs on IMF7. For the ICEEMDAN, IMF 1 and 2 are spurious residual noise modes. The sum of these 4 IMFs shows that the maximum amplitude of the residual noise is about 0.001. Mode A is split into IMF 3 and 4. Mode B is split into IMF 5 and 6. As observed from Fig. 12(b) and (c), the EEMD, EEMD, and ICEEMDAN underestimate the amplitude of Mode B because of mode splitting. In addition, the EEMD/CEEMD results cannot match both the amplitude and phase of Mode C. TABLE 5 lists the *MMSI*s of different methods. As can be seen, the UPEMD significantly reduces the mode splitting as compared to the noise-assisted methods.

For the condition with $\varepsilon = 0.1$, the UPEMD with $n_p = 32$ provides the close solutions for Modes A and B, but not Mode C. In contrast, the noise-assisted derived IMFs do not match any of the expected physical modes.

Example 6 (Analysis of Blood Flow Velocity):

A brain blood flow velocity (BFV) signal [24] used to assess dynamic cerebral autoregulation (CA) is shown in Fig. 13 (a). The data is 40-sec long and sampled at 50Hz rate. As discussed previously [3], the spontaneous BFV oscillation is entrained by respiration over the frequency range of 0.18 $\sim$ 0.3 Hz. The signals decomposed by different disturbance-assisted EMDs are shown in Fig. 13 (a). The respiratory oscillation mode (RO mode) appears in IMF 6 for EEMD/CEEMD, while appears in IMF 7 for ICEEMDAN and UPEMD. The *PMSI* values displayed in Fig. 13(b) are adopted to measure the mode splitting effect between different methods. It shows that the UPEMD method suppresses the mode splitting phenomenon better than the other methods do. In addition, the *PMSI* values for UPEMD with 2 and 32 phases are quite close indicating that mode splitting is insensitive to the number of phases in UPEMD.

In the disturbance-assisted EMDs, the resultant IMFs are obtained by averaging the respective IMFs over different realizations. Thus the IMF may violate the IMF conditions [5] that provides as an index to examine the performance of different EMD-based methods. Here we investigate the waveforms of the RO mode by different methods. The RO modes for the ICEEMDAN and UPEMD with $n_p = 32$ both satisfy the IMF conditions. The waveform is distorted for UPEMD with $n_p = 2$ around $t = 22$ sec (with a negative maximum) and 36 sec (with a positive minimum), and are distorted for EEMD and CEEMD around $t = 11$ sec (with a negative maximum).

Example 7 (Analysis of Speech Signal):

A speech signal of a man pronouncing "A ship was torn apart" sampled at 16 kHz is shown in Fig. 14(a). The period $t = 0.75$ to 0.79 sec corresponding to the consonant "s" is enlarged and shown in the top panel of Fig. 14(c). Strong mode mixing occurs in the IMFs obtained from the standard EMD. As discussed previously, in the EEMD, the data cannot be exactly reconstructed from the IMFs, thus hissing-like audible residual noise appears in periods without speech. Therefore IMFs obtained by UPEMD are compared to those obtained by the CEEMD and ICEEMDAN. The IMFs are shown in Fig. 14(c) to (e), respectively.

There are some positive minima and negative maxima in IMF 2 and 3 obtained by CEEMD, and in IMF2 obtained by ICEEMDAN. This can be interpreted as the mode mixing because the amplitude of the disturbance is too small, or the mode splitting that an IMF consists of different copies of scales as discussed in Sec. 3. We also observe waveform distortion in IMF3 obtained by CEEMD, and in IMF 4, 5, and 6 obtained by UPEMD with $n_p = 2$, and in IMF 5 obtained by UPEMD with $n_p = 32$. Obviously, the UPEMD effectively suppresses mode splitting as compared to CEEMD and ICEEMDAN that can be also examined the *PMSI* values in Fig. 14(b).

The Hilbert spectrums of different methods are displayed in Fig. 14(f) to (g). The violation of the IMF conditions may lead to negative frequency and is not displayed in the figure. In the time-frequency picture obtained by each EMD-based algorithm, the residual noise effect makes the instantaneous frequency fluctuate around the exact value, while the mode splitting effect makes the two adjacent frequency components move close to each other or even overlap. These two effects then make the time-frequency picture looks blurry and the blurriness (sharpness) of the picture can be used to compare the performance of different EMD-based algorithms. As can

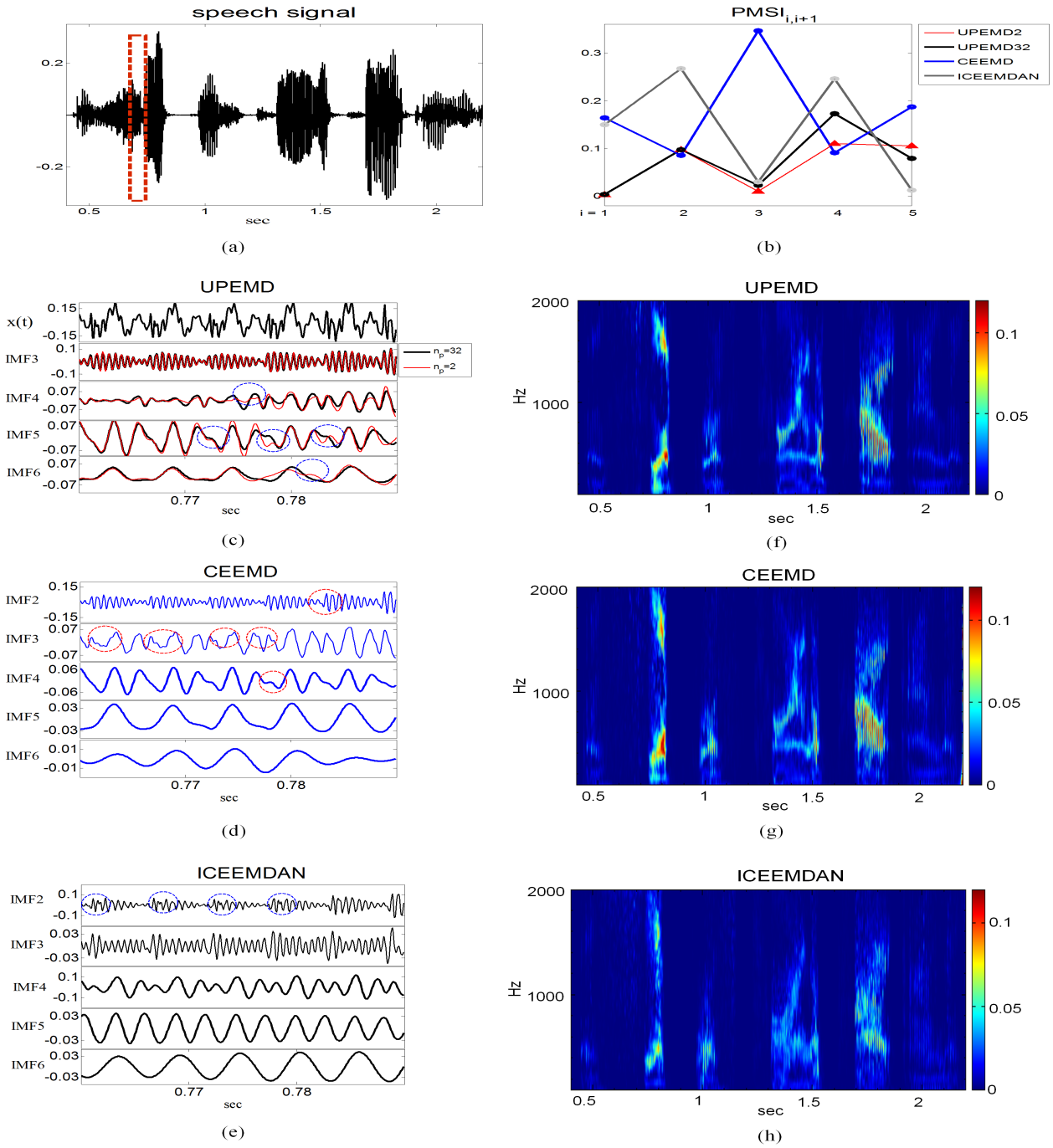

FIGURE 14. Analysis of the speech signal in Example 7 using different disturbance-assisted EMDs with $\varepsilon = 1$ and $n_s = 10$. (a) The signal, where the period between $t = 0.75$ to 0.79 sec is marked in the rectangle; (b) the *PMSI* values using different EMD-based methods; (c) the IMFs obtained by UPEMD with $n_p = 32$; (d) the IMFs obtained by CEEMD with $n_e = 200$, (e) the IMFs obtained by ICEEMDAN with $n_e = 200$. The points with positive local minima or negative local maxima are marked in the circles. (f) the Hilbert spectrogram of the IMFs obtained by UPEMD; (g) the Hilbert spectrogram of the IMFs obtained by CEEMD with $n_p = 32$; (h) the Hilbert spectrogram of the IMFs obtained by ICEEMDAN.

be seen that the Hilbert spectrums obtained by CEEMD and ICEEMDAN are more blurred than that by UPEMD with $n_p = 32$.

VII. CONCLUSIONS

The class of the disturbance-assisted EMDs including noise-assisted and masking EMD can resolve the mode mixing problem that is inherent in the standard EMD algorithm. It is known that noise-assisted EMD may introduce two side effects: mode splitting and residual noise. We further demonstrate in this study that the masking EMD also suffers from these two effects. In addition, we show that mode splitting leads to an underestimation of the amplitude of the physical components while residual noise contaminates the data and

generates oscillatory components with distorted waveforms (i.e., incorrect IMFs without true physical meanings). Mode splitting is, on average, much more severe in the noise-assisted EMD as compared to the masking EMD. The effect of residual noise on the noise-assisted EMD results can be reduced by increasing the number of realizations but at the cost of much longer computational time.

To improve the EMD performance, we propose a new disturbance-assisted EMD: UPEMD, in which a series of assisted sinusoids with uniformly distributed phases are used to resolve the serious residual noise problem. By considering a signal with two oscillatory components, we show that the level of residual noise is continuously reduced as the number of sinusoids increases. The noise is substantially suppressed when using 4 to 32 assisted sinusoids. Moreover, the mode splitting effect is insensitive to the number of sinusoids. Note that this method is a generalization of the masking EMD introduced by Deering and Kaiser, in which positive and negative pairs of sinusoids are used as the assisted disturbance.

By further considering a generic case where data is decomposed into multiple IMFs, we propose the multi-level version of the UPEMD. We tested UPEMD using numerical simulations with stationary, nonstationary, nonlinear and real-world data sets, and we found that the new method not only resolves the mode mixing problem in the EMD, but also has substantially reduced mode-splitting effect in the noise-assisted EMD. More importantly, the new method minimizes/removes the unphysical residual noise in the masking EMD. Last but not the least, UPEMD is a computationally efficient method and can be readily utilized in a real-time manner in modern microcontroller (MCU) to resolve many scientific and engineering problems.

ACKNOWLEDGMENT

The authors thank Melissa Patxot and Tommy To at Brigham & Women's Hospital/Harvard Medical School for English editing.

REFERENCES

[1] N. E. Huang *et al.*, "The empirical mode decomposition and the Hilbert spectrum for nonlinear and non-stationary time series analysis," *Proc. R. Soc. Lond. A, Math. Phys. Sci.*, vol. 454, no. 1971, pp. 903–995, Mar. 1998.

[2] Y. H. Wang, H.-W. V. Young, and M.-T. Lo, "The inner structure of empirical mode decomposition," *Phys. A, Stat. Mech. Appl.*, vol. 462, pp. 1003–1017, Nov. 2016.

[3] M.-T. Lo, V. Novak, C.-K. Peng, Y. Liu, and K. Hu, "Nonlinear phase interaction between nonstationary signals: A comparison study of methods based on Hilbert–Huang and Fourier transforms," *Phys. Rev. E, Stat. Phys. Plasmas Fluids Relat. Interdiscip. Top.*, vol. 79, no. 6, p. 061924, Jun. 2009.

[4] N. E. Huang, Z. Shen, and S. R. Long, "A new view of nonlinear water waves: The Hilbert spectrum," *Annu. Rev. Fluid Mech.*, vol. 31, pp. 417–457, Jan. 1999.

[5] Z. Wu and N. E. Huang, "Ensemble empirical mode decomposition: A noise-assisted data analysis method," *Adv. Adapt. Data Anal.*, vol. 1, no. 1, pp. 1–41, 2008.

[6] J. R. Yeh, J. S. Shieh, and N. E. Huang, "Complementary ensemble empirical mode decomposition: A novel noise enhanced data analysis method," *Adv. Adapt. Data Anal.*, vol. 2, no. 2, pp. 135–156, 2010.

[7] M. E. Torres, M. A. Colominas, G. Schlotthauer, and P. Flandrin, "A complete ensemble empirical mode decomposition with adaptive noise.," in *Proc. IEEE Int. Conf. Acoust., Speech, Signal Process. (ICASSP)*, Prague, Czech Republic, May 2011, pp. 4144–4147.

[8] M. A. Colominas, G. Schlotthauer, and M. E. Torres, "Improved complete ensemble EMD: A suitable tool for biomedical signal processing," *Biomed. Signal Process. Control*, vol. 14, pp. 19–29, Nov. 2014.

[9] R. Deering and J. F. Kaiser, "The use of a masking signal to improve empirical mode decomposition," in *Proc. IEEE Int. Conf. Acoust., Speech, Signal Process. (ICASSP)*, Philadelphia, PA, USA, vol. 4, Mar. 2005, pp. iv/485–iv/488.

[10] N. Senroy, S. Suryanarayanan, and P. F. Ribeiro, "An improved Hilbert–Huang method for analysis of time-varying waveforms in power quality," *IEEE Trans. Power Syst.*, vol. 22, no. 4, pp. 1843–1850, Nov. 2007.

[11] D. S. Laila, A. R. Messina, and B. C. Pal, "A refined Hilbert–Huang transform with applications to interarea oscillation monitoring," *IEEE Trans. Power Syst.*, vol. 24, no. 2, pp. 610–620, May 2009.

[12] X. Hu, S. Peng, and W.-L. Hwang, "EMD revisited: A new understanding of the envelope and resolving the mode-mixing problem in AM-FM signals," *IEEE Trans. Signal Process.*, vol. 60, no. 3, pp. 1075–1086, Mar. 2012.

[13] Y. Yang, J. Deng, and D. Kang, "An improved empirical mode decomposition by using dyadic masking signals," *Signal Image Video Process.*, vol. 9, no. 6, pp. 1259–1263, Sep. 2015.

[14] W.-C. Shen, Y.-H. Chen, and A.-Y. Wu, "Low-complexity sinusoidal-assisted EMD (SAEMD) algorithms for solving mode-mixing problems in HHT," *Digit. Signal Process.*, vol. 24, pp. 170–186, Jan. 2014.

[15] H. Hong, X. Wang, and Z. Tao, "Local integral mean-based sifting for empirical mode decomposition," *IEEE Signal Process. Lett.*, vol. 16, no. 10, pp. 841–844, Oct. 2009.

[16] N. ur Rehman and D. P. Mandic, "Filter bank property of multivariate empirical mode decomposition," *IEEE Trans. Signal Process.*, vol. 59, no. 5, pp. 2421–2426, May 2011.

[17] G. Rilling and P. Flandrin, "One or two frequencies? The empirical mode decomposition answers," *IEEE Trans. Signal Process.*, vol. 56, no. 1, pp. 85–95, Jan. 2008.

[18] P. Flandrin, G. Rilling, and P. Goncalves, "Empirical mode decomposition as a filter bank," *IEEE Signal Process. Lett.*, vol. 11, no. 2, pp. 112–114, Feb. 2004.

[19] P. Flandrin, P. Gonçalvès, and G. Rilling, "EMD equivalent filter banks, from interpretation to applications," in *Hilbert-Huang Transform and Its Applications*, N. E. Huang and S. S. P. Shen, Eds. Singapore: World Scientific, 2005, pp. 57–74.

[20] J. Gilles, "Empirical wavelet transform," *IEEE Trans. Signal Process.*, vol. 61, no. 16, pp. 3999–4010, Aug. 2013.

[21] N. Rehman and D. P. Mandic, "Multivariate empirical mode decomposition," *Proc. R. Soc. Lond. A, Math. Phys. Sci.*, vol. 466, no. 2117, pp. 1291–1302, Apr. 2010.

[22] M.-T. Lo *et al.*, "Method and system for extracting ventricular fibrillation signals in electrocardiogram using spline interpolation with uniform phase ensembles," U.S. Patent 9 451 898 B2, Jul. 2, 2014.

[23] Y.-H. Wang, C.-H. Yeh, H.-W. V. Young, K. Hu, and M.-T. Lo, "On the computational complexity of the empirical mode decomposition algorithm," *Phys. A, Statist. Mech. Appl.*, vol. 400, pp. 159–167, Apr. 2014.

[24] K. Hu *et al.*, "Nonlinear pressure-flow relationship is able to detect asymmetry of brain blood circulation associated with midline shift," *J. Neurotrauma*, vol. 26, no. 2, pp. 227–233, Feb. 2009.

YUNG-HUNG WANG received the Ph.D. degree in aeronautics and astronautics from Stanford University, Stanford, CA, USA, in 1998. He is currently an Associate Research Fellow with the Research Center for Adaptive Data Analysis, National Central University, Taiwan. His research interests include signal processing, biomedical engineering, electronic design automation, and fluid mechanics.

KUN HU received the Ph.D. degree in statistical physics from Boston University, Boston, MA, USA, in 2005. Then, he received his multidisciplinary post-doctoral training in human physiology, neuroscience, and system biology with the Harvard Medical School, Boston.

He is currently an Associate Professor of medicine with the Harvard Medical School, and a Physiologist and the Director of the Medical Biodynamics Program, Brigham and Women's Hospital, Boston. His research interests include behavioral, cardiovascular, and circadian/sleep regulations in health and disease.

Dr. Hu is a member of the American Academy of Sleep Medicine, the Sleep Research Society, the Society for Neuroscience, and the International Cerebral Autoregulation Research Network Committee.

MEN-TZUNG LO received the Ph.D. degree in communication engineering from National Taiwan University with a focus on biomedical signal and image processing as well as biomedical imaging and drug delivery systems.

He received his post-doctoral training with the Taipei Veteran General Hospital and the Syncope and Falls in the Elderly Laboratory, Beth Israel Deaconess Medical Center, Harvard Medical School, for applying novel nonlinear signal analysis to multiple biomedical signals from different disease groups to explore their underlying properties and quantifying the properties altered from a normal as parameters for severity or prognosis of diseases. He is currently a Professor with the Department of Biomedical Sciences and the Institute of Translational and Interdisciplinary Medicine, Engineering National Central University, Taiwan. His two main research interests are time-varying interactions between multiple biological signals of human subjects, and the changes of nonlinear properties in different physiological and pathological statuses.